ACS APPLIED MATERIALS & INTERFACES

Research Article

www.acsami.org

Lasing Behavior Modulation for ZnO Whispering-Gallery Microcavities

Gangyi Zhu,[†] Chunxiang Xu,*[,†] Lisha Cai,[‡] Jitao Li,[†] Zengliang Shi,[†] Yi Lin,[†] Guofeng Chen,[†] Tao Ding,[†] Zhengshan Tian,[†] and Jun Dai[†]

[†]State Key Laboratory of Bioelectronics, School of Electronic Science and Engineering, Southeast University, Nanjing 210096, China

[‡]National Laboratory of Solid State Microstructures, Nanjing University, Nanjing 210016, China

ABSTRACT: Four configurations of whispering-gallery-mode (WGM) microcavities were designed and fabricated to modulate the optically pumped lasing characteristics by polymer modification on hexagonal ZnO microrod surfaces. On the basis of the total internal reflection (TIR) at the boundary of microcavities, the lasing characteristics were improved by raising the relative refractive index. Considering the different reflective conditions at various side surfaces, the typical lasing mode equation for whispering-gallery microcavity was modified to adapt for general situation even with unsymmetrical structure, and then employed to discuss the observed lasing behaviors, in the polyvinylcarbazole (PVK) modified ZnO microrods, such as mode position, mode numbers and quality factor. The optical field distributions for TE modes of the four configurations were also simulated by 2-dimensional finite difference time-domain (FDTD) method. The simulation agreed well with the experimental results to support the resonance mechanism.

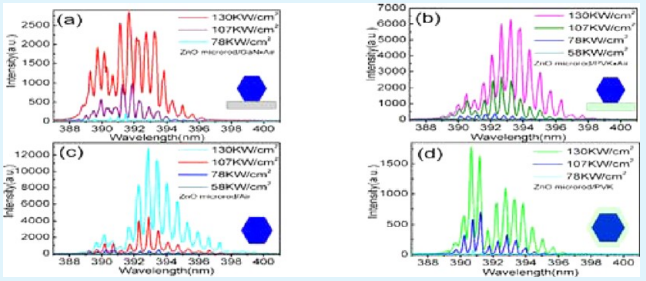

KEYWORDS: *whispering-gallery-mode, hexagonal ZnO microrod, total internal reflection, relative refractive index, polyvinylcarbazole, finite difference time-domain method*

1. INTRODUCTION

As a wide direct bandgap (3.37 eV) semiconductor with a large exciton binding energy (60 meV) at room temperature (RT), ZnO has been thought of the most promising candidate material for short-wavelength optoelectronic devices, especially for ultraviolet (UV) lasers. The UV lasing in ZnO material has attracted tremendous attention since the first report in 1997.[1] To date, optically and electrically pumped lasing in various ZnO micro/nanostructures have been observed.[2−10] According to the resonant cavity structures, those reported lasing actions can be classified as random,[5−7] Fabry−Perót (F−P),[8,9] and WGM lasing.[4,10] Among them, the WGM lasing shows much higher quality factor (Q) and lower lasing threshold because of its extremely weak optical loss of the TIR at the cavity boundary For examples, C. Czekalla[2] and J. Dai[3] have reported WGM lasing with Q factor more than 3000 in ZnO microrod at low and room temperature, respectively. In our previous work,[10] the ZnO microrod/p-GaN heterostructured laser diode has been fabricated and the electrically pumped WGM laser has been observed. However, the electrically pumped lasing has a much lower Q than the corresponding optically pumped lasing because of the non-negligible optical loss on ZnO/GaN interface, where the light can not be reflected totally due to the close refractive index of ZnO and GaN. So it is required to improve the lasing performance through interface modification. It is also expected to create chemical/biological sensors on TIR[11,12] because the WGM lasing behaviors are sensitive to the surface modification. Therefore, it is worth to understand the lasing behaviors of the WGM microcavity when its side surfaces are covered by other mediums. In this paper, four different configurations of ZnO-based WGM microcavities were designed to modulate the optically pumped lasing behaviors, such as lasing modes, Q factor and threshold. The lasing characteristics and resonance mechanism, especially the relationship between the lasing mode and the relative refractive index n_r, were systematically discussed in both experiment and theory. Correspondingly, the TE optical field distributions in these cavities were also simulated to illustrate the resonant process by a 2-dimensional FDTD method. It should be pointed out that the lasing mode number equation used in all previous reports[2,3,13,14] is only suitable for the WGM cavity with symmetrical distribution of reflective index, such as air-sounded hexagonal ZnO microrod. In this study, the equation was modified to be fitted to the general situation, for example, the ZnO microrod is asymmetrically coated by PVK and air. PVK is selected as a kind of p-type polymer semiconductors, which can be used as a buffer layer to construct a ZnO microrod/p-GaN heterojunction for electro-pumped WGM laser.

Received: August 27, 2012
Accepted: October 18, 2012
Published: October 18, 2012

2. EXPERIMENTAL SECTION

An individual ZnO microrod, which was grown by vapor-phase transport on a silicon substrate as our previously reported,[3,10] was employed as a WGM cavity with and without PVK modification. The SEM image of the as-grown ZnO microrods in Figure 1 shows the size of with about 10 μm in diameter.

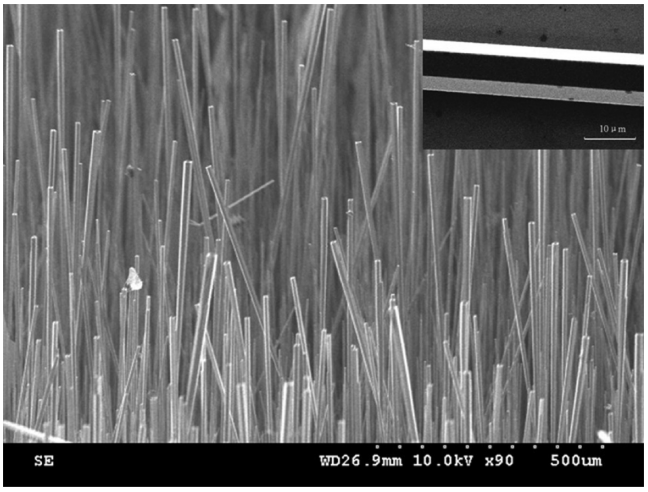

Figure 1. SEM image of ZnO microrods inserted with an enlarged individual one.

The inserted SEM image of an enlarged individual microrod exhibits the perfect hexagonal cross section and smooth side surfaces, which is beneficial to form a natural microcavity for WGM lasing with low threshold, distinct modes and definite lasing output directions.[2−4] SEM images were recorded using a Hitachi scanning electron microscope S-3000N.

Figure 2a illustrates the four schematic configurations of WGM microcavities in top-view, side-view and the SEM images of the ZnO microrod on different substrates. Sample I has a ZnO microrod/GaN·Air structure. One side surface of an individual ZnO microrod with diameter D = 9.8 μm is closely fixed on a cleaned GaN (n_{GaN} = 2.49) substrate, where the n_r = n_{ZnO}/n_{GaN} = n_{ZnO}/2.49 The refractive index of PVK and GaN is assumed as fixed values due to their change is very small in our discussed wavelength range of 385−400 nm. The other five side surfaces of the ZnO microrod are bare in air, where the n_r is all equal to n_{ZnO}. Sample II has a ZnO microrod/PVK·Air structure. The PVK films were deposited by spinning coating the chloroform solution of 4 mg/mL PVK on the cleaned GaN substrate using a KW-4A Spin Coater. The ZnO microrod was transferred onto a PVK (n_{PVK} =1.683) substrate. One side surface of the ZnO microrod is closely contact with the PVK film, where n_r is n_{ZnO}/1.683′ and the other five side surfaces have n_r of n_{ZnO}. Sample III has a ZnO microrod/air structure. The same ZnO microrod was directly bare in air (n_{Air} = 1). The all side surfaces have n_r of n_{ZnO}. Sample IV has a ZnO microrod/PVK structure. The ZnO microrod were vertically dipped into the chloroform solution of 2 mg/mL PVK, and then vertically pulling out, consequently, the all six side surfaces were all coated by PVK thin film. The ZnO microrod was surrounded by PVK film through dip-coating method. All side surfaces have n_r of n_{ZnO}/1.683.The optical measurement was carried out as the schematic geometry in Figure 2b, similar to our previous report.[13] A nanosecond pulse Nd:YAG laser operating at 355 nm was focused and irradiated onto the ZnO microrod with the incident angle of about 60° to one side surface of the microrod. The emission signal was collected by a fiber and coupled into a charge-coupled-device (CCD) array detector in an optical-multichannel analysizer (OMA) system. The collect facet of the fiber was adjusted to orientate to the direction with the strongest optical signal. It is noted that only one ZnO microrod was used to modify with different medium forming the above four samples.

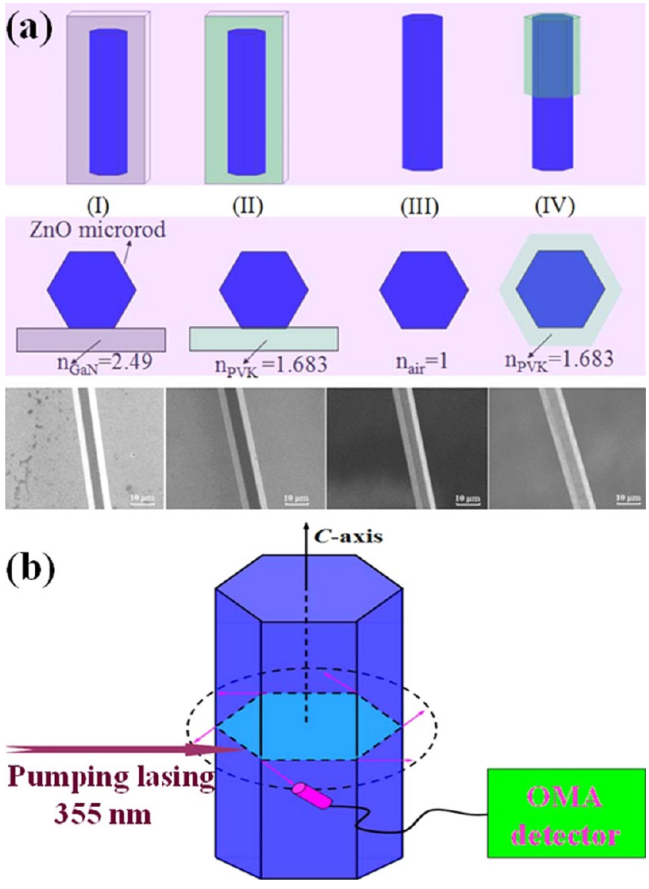

Figure 2. (a) Schematic diagrams of four WGM microcavities in top-view, side-view, and the SEM images of the ZnO microrod on different substrates: (I) ZnO microrod/GaN·Air; (II) ZnO microrod/PVK·Air; (III) ZnO microrod/Air; and (IV) ZnO microrod/PVK. (b) The schematic diagram for the lasing detection.

3. RESULTS AND DISCUSSION

Lasing Behaviors Modulation. Figure 3a−d display the emission spectra of the four samples at various excitation power densities. From the serial spectra, it can be seen that the lasing characteristics, such as the threshold, increasing rate of the lasing intensity, mode number and position, are modulated depending on the variation of the external mediums at the cavity boundaries. The detailed behaviors are described and discussed as following.

The stimulated emission generated in each cavity with the different excitation thresholds. Figure 3e plots the lasing emission intensity versus the excitation power density. It can be seen that the lasing threshold is about 70, 60, 50, and 78 KW/cm^2 for samples I, II, III, and IV, respectively. When the excitation power density exceeds the respective threshold, the lasing spectral emission intensities increase rapidly. The increasing rate of stimulated emission intensity is in the

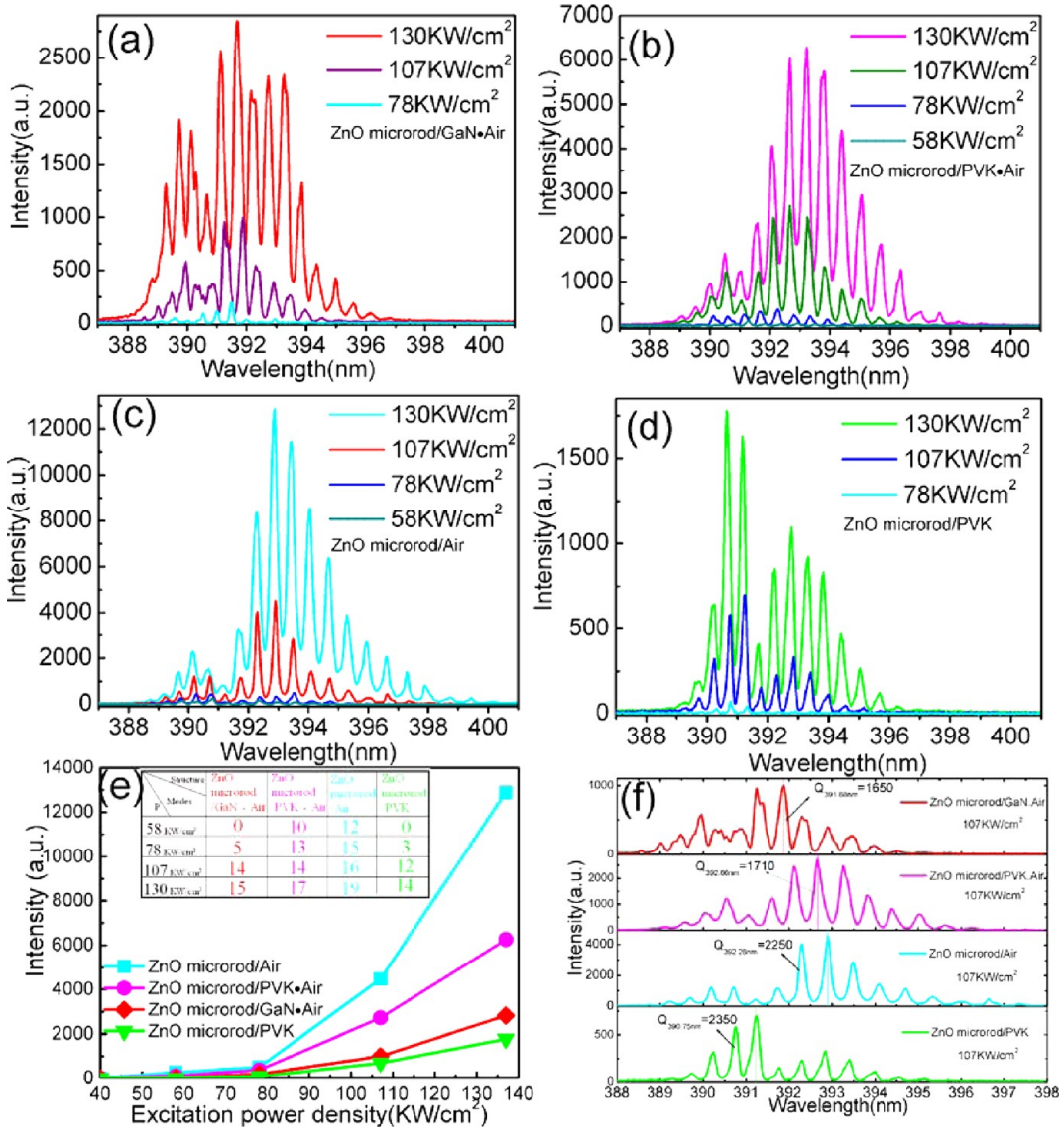

Modes \ Structure	ZnO microrod / GaN - Air	ZnO microrod / PVK - Air	ZnO microrod / Air	ZnO microrod / PVK
58 KW/cm²	0	10	12	0
78 KW/cm²	5	13	15	3
107 KW/cm²	14	14	16	12
130 KW/cm²	15	17	19	14

Figure 3. (a–d) Lasing spectra under different excitation power densities for sample I, II, III, and IV, respectively, (e) the lasing emission intensity versus the excitation power density inserted the statistic lasing mode numbers and threshold values in the table, and (f) representative lasing spectra and corresponding *Q* factors under the excitation power density of 107 KW/cm^2.

sequence of sample IV < I<II < III, so the four samples present different emission intensity at the same excitation power density. The sequence of the threshold and intensity increasing rate also indicate the optical quality of these four microcavities. With increase of the excitation power, more lasing modes obtain sufficient gain to overcome the loss. The four samples present the various numbers of the lasing modes as shown the inserted table in Figure 3e. For example, at the excitation power density of 107 KW/cm^2, the lasing mode numbers of sample I, II, III, and IV are 15, 17, 19 and 14, respectively. When the excitation power density is higher than 107 KW/cm^2, the lasing mode numbers keep the same order of sample IV < I<II < III.

These behaviors of threshold, mode numbers, lasing intensity and its increasing rate are ascribed to the various TIR efficiency at the cavity boundaries for the different samples. According to the TIR theory, the higher n_r of the microcavities indicates the better TIR and the weaker optical loss in ZnO microrod, and then deduce the stronger lasing emission, the faster increasing rate, and the lower lasing threshold. Sample I, II, and III have the same five interfaces of ZnO/air, and one different interfaces of ZnO/GaN, ZnO/PVK, and ZnO/air, where n_r increases from $n_{ZnO}/2.49$ to $n_{ZnO}/1.683$ to $n_{ZnO}/1$ Therefore, the threshold reduces lower and lower, and the lasing intensity increase faster and faster in order of sample I, II and III. In the same way, the threshold increases and lasing intensity enhancement becomes slowly because of n_r reduce when the ZnO microrod was surrounded by PVK in stead of air from sample III to sample IV.

The lasing mode position is sensitively modulated by n_r at the cavity boundary. As shown the representative spectra of the four samples pumped at 107 KW/cm^2 in Figure 3f, the strongest mode is at about 391.88, 392.66, 392.93, and 391.24 nm for sample I, II, III, and IV, respectively. It is attributed to the alteration of phase angle because of the n_r variation at the side surfaces. The phase angle of the reflective light is changed relative to the incident light as it is totally reflected at the side surfaces of ZnO microrod. Such phase shift induces the modulation of the resonant peaks. The influence of the coated PVK on the phase angle and further on the lasing modes are

dx.doi.org/10.1021/am301800k | ACS Appl. Mater. Interfaces 2012, 4, 6195–6201

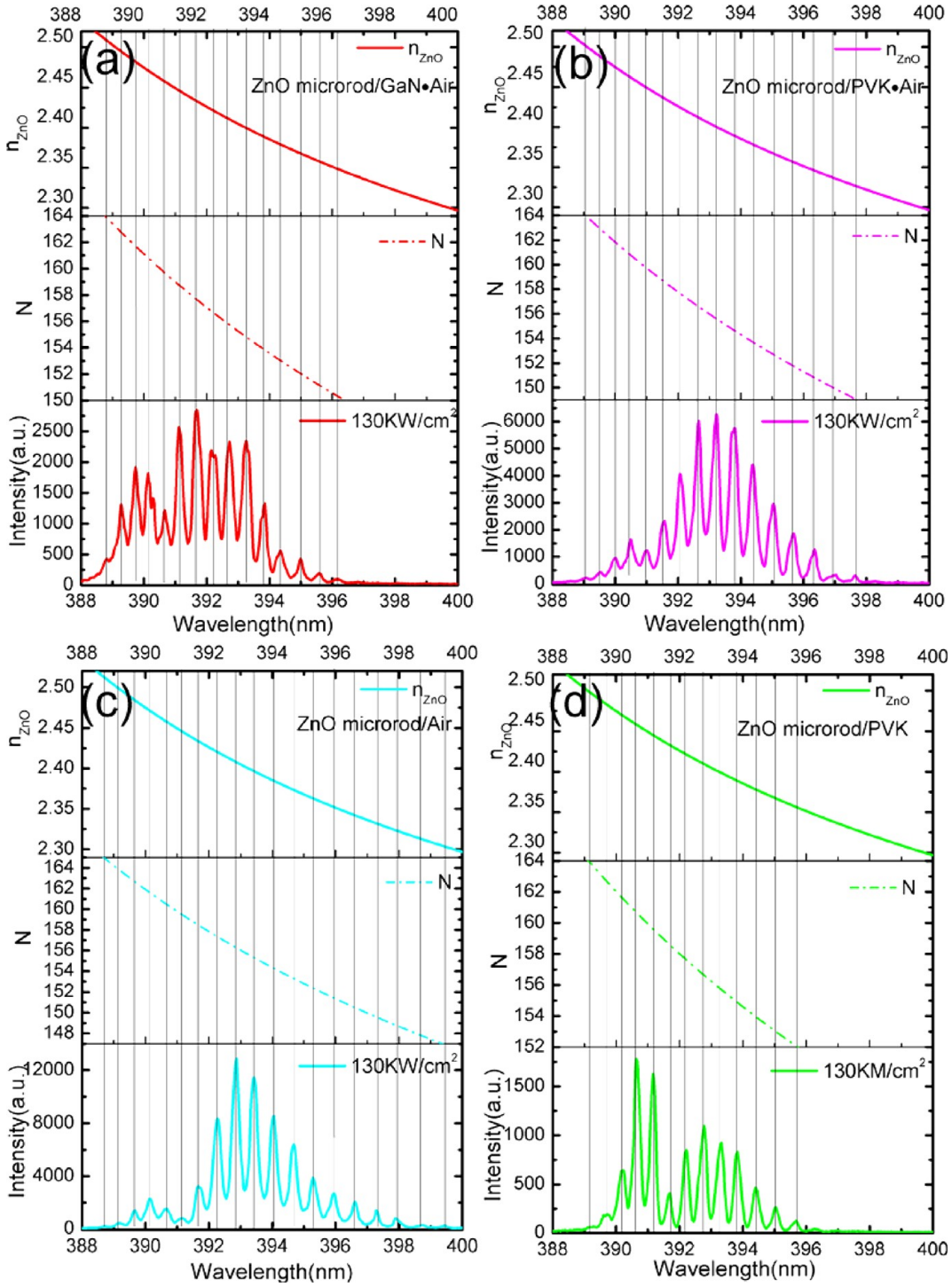

Figure 4. ZnO dispersion relations (top), simulated lasing modes and the corresponding serial numbers according to the modified mode equation (middle), and the lasing spectra at excitation power density of 130 KW/cm^2.

discussed in detail through the modified mode equation in the next section.

It is also noted that the lasing modes presents two envelops at 390 and 393 nm, as show the Figure 3a–d. This phenomenon is assumed to the interaction among the excitons. High exciton concentration would be generated as enhancing of the excitation intensity or improving the excitation efficiency, which would result in the red-shift of the emission band because of the reduced system energy. Among four configurations, the higher n_r of the microcavities indicates better excitation efficiency in ZnO microrod. At the same excitation power density, the intensity of the 393 nm envelop relative to that of the 390 nm envelop is improved in order of sample IV, I, II, and III, as shown in Figure 3(a–d), in which the excitation efficiency from sample IV, I, and II to III is increased because of the modified n_r. This phenomenon is very obvious for sample IV and sample III, which are surrounded by PVK and air, respectively. The excitation efficiency of sample III is higher than that of sample IV, this result in higher exciton concentration in ZnO/air microcavity than that in ZnO/PVK

dx.doi.org/10.1021/am301800k | ACS Appl. Mater. Interfaces 2012, 4, 6195–6201

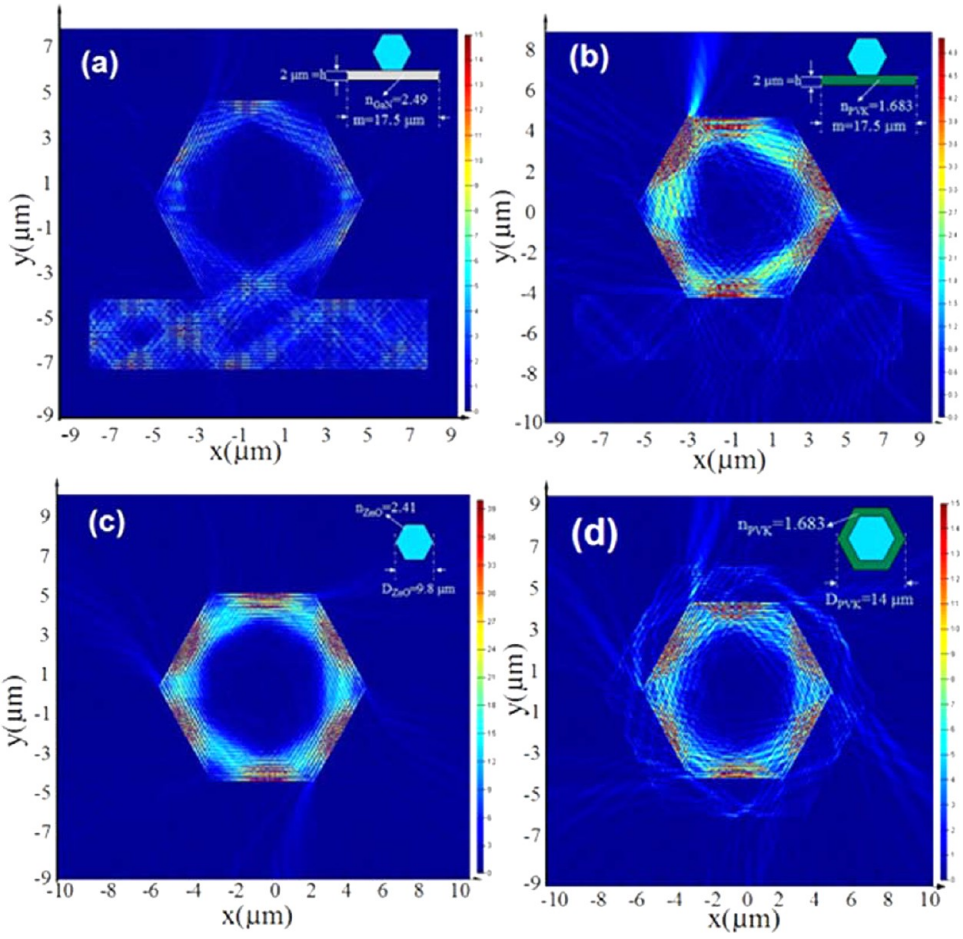

Figure 5. Simulated optical field distributions of the TE modes for the inserted WGM microcavities, the linear false color scale displayed the strength of the TE field.

microcavity under the same excitation power. It is obviously seen that the intensity of the 393 band relative to 390 band of sample III is much stronger than that of sample IV.

Lasing Mode Number Equation. As a birefringent material with wurtzite structure, the TM polarized mode in UV range from ZnO microcavity is extremely weak and difficult to be detected comparing with the TE mode, so we just discuss the TE mode here. The refractive index for TE polarization light can be expressed using Sellmeier's dispersion function:[2,3]

$$n_{\mathrm{ZnO}}(\lambda) = \left(1 + \frac{2.4885\lambda^2}{\lambda^2 - 102.30^2} + \frac{0.215\lambda^2}{\lambda^2 - 372.60^2} + \frac{0.2550\lambda^2}{\lambda^2 - 1850^2}\right)^{1/2} \quad (1)$$

where $n_{\mathrm{ZnO}}(\lambda)$ represents the ZnO refractive index at wavelength of λ. According to the Fresnel formula, the phase-shift of TIR can be expressed as $\phi = \tan^{-1}(\beta(3n_r^2 - 4)^{1/2})$. For the hexagonal WGM resonance, $N\pi = 3\sqrt{3}nD/2\lambda\ \pi - 6\phi$ so the relationship between the resonant wavelength λ and the corresponding mode serial number N can be deduced as[2−4,13,14]

$$N = \frac{\frac{3\sqrt{3}}{2}Dn_{\mathrm{ZnOO}}}{\lambda} - \frac{6}{\pi}\tan^{-1}(\beta\sqrt{3n_r^2 - 4}) \quad (2)$$

where D is the circum circle diameter of hexagonal microcavity and n_r is the relative refractive index of ZnO microrod to the outside medium. The factor β are equal to n_r^{-1} and n_r for TM and TE polarization, respectively. The second term on the right hands is related to phase-shift of TIR at the six side surfaces.

However, eq 2 is only suitable for hexagonal ZnO microcavity symmetrically coated by only one type of medium, such as sample III. In sample I and II, the ZnO microrod is asymmetrically coated by different medium. In this case, the phase-shift of ZnO/GaN (or PVK) interfaces is different from that of other five ZnO/air ones. Here, we proposed a universal equation to calculate the lasing modes and serial numbers of the hexagonal WGM cavity:

$$N = \frac{3\sqrt{3}\,n_{\mathrm{ZnO}}D}{2\lambda} - \sum_{i=1}^{6}\frac{1}{\pi}\tan^{-1}(n_{ri}\sqrt{3n_{ri}^2 - 4}) \quad (3)$$

where $n_{ri} = n_{\mathrm{ZnO}}/n_i$ represents n_r at the ith side surface of the modified ZnO microrod and n_i denotes the refractive index of the corresponding medium.

For sample I, n_r of the ZnO microrod relative to GaN is $n_{\mathrm{ZnO}}/2.49$. This determines partial reflection at the interface of ZnO/GaN. It is estimated the Brewster angle θ_B = arctan 2.49/2.41 = 46° at this interface, which is smaller than the incident angle of 60° for the WGM resonance. According to Fresnel formula and Brewster law of optical waves, the light phase would be altered π as it was reflected at ZnO/GaN interface.

dx.doi.org/10.1021/am301800k | ACS Appl. Mater. Interfaces 2012, 4, 6195−6201

Considering the total phase shift from the interface of ZnO/GaN and the other five side surfaces, eq 3 can be rewritten as

$$N = \frac{3\sqrt{3}\,n_{ZnO}D}{2\lambda} - \frac{5}{\pi}\tan^{-1}\left(n_{ZnO}\sqrt{3{n_{ZnO}}^2 - 4}\right) - \frac{1}{\pi} \times \pi = \frac{3\sqrt{3}\,n_{ZnO}D}{2\lambda} - \frac{5}{\pi}\tan^{-1}\left(n_{ZnO}\sqrt{3{n_{ZnO}}^2 - 4}\right) - 1 \quad (4)$$

According to eq 4, the WGM lasing modes and the corresponding serial numbers N are simulated and illustrated in Figure 4. The experimental lasing spectra excited at 130 KW/cm^2 are also displayed in figure 4 for comparison. The lasing modes can be indexed as serial numbers from 151 to 164 for sample I, 149−164 for sample II, 147−165 for sample III, and 151−164 for sample IV, respectively. The dashed line described the relationship of N with wavelength λ. The intersections of the vertical lines and dispersion curve (top solid line) and $N - \lambda$ line (middle dashed one) reveal the integer serial numbers, refractive index and corresponding lasing peaks, respectively. The lasing mode appears at different position for different samples due to the variation of phase angle with n_r. It is obviously seen that the simulated resonant wavelength agree with the experimental lasing modes very well.

Simulated Optical Field Distribution. To further study the lasing behaviors, a commercial 2-dimensional FDTD software was employed to simulate the optical field distributions of the TE modes in the microcavities.[15,16] The insets in Figure 5 display structural parameters of the four configurations corresponding to the diagrams in Figure 2. For this simulation, a Gaussian beam with fwhm of 8 nm centered at 393 nm was set as the light source, which matches with the near-band emission of the ZnO microrod. The refractive index of ZnO microrod is regards as 2.41, which corresponds to the value at 393 nm.

The simulation results are shown in figure 5. It can be seen from Figure 5a that the light leaks seriously from the ZnO microrod to the GaN film because the TIR condition is not satisfied at the interface of ZnO/GaN. Even so, the light can still be confined effectively by the other five side surfaces of ZnO/air and generate the sufficient resonance. When the GaN film is replaced by PVK, as shown in Figure 5b, the heavy optical loss is shut immediately. The majority of the light takes place TIR in hexagonal ZnO microrod to generate resonance and then emits out from the corners of hexagonal microcavity.[17,18] For sample II, the TIR angle (44.3°) at ZnO/PVK interface is bigger than that (24.5°) at the other five ZnO/air interfaces, which suggested lower TIR efficiency at the interface of ZnO/PVK, so a little of TE light transmits from the ZnO microrod to the PVK film. Naturally, the light is confined more efficiently in the cavity when the all six side surfaces are surrounded by air with low reflective index, as shown in Figure 5c.

It is easy to understand that the some lasing performance of sample IV, such as threshold, is not as good as that of sample III because n_r of ZnO/PVK is lower than that of ZnO/air. However, the simulation result in Figure 5d exhibits an interesting phenomenon. A part of light is confined in the PVK layer outside of ZnO microcavity, which should be beneficial to improve some lasing property, such as Q factor discussed following.

Lasing *Q* Factor. The lasing quality, Q, is calculated according to the definition $Q = \lambda/\Delta\lambda$ where λ is the peak wavelength and $\Delta\lambda$ is the fwhm. From the spectra in Figure 3f, the Q factors are estimated as 1650, 1710, and 2250 for sample I, II, and III, respectively. The gradually increased Q value is attributed to the improvement of the light TIR on side surfaces of ZnO microrod with n_r increase. It is interesting to note that the highest lasing Q factor of 2350 is obtained from sample IV when the six side surfaces of the ZnO microrod are coated by PVK instead of air in sample III and n_r reduces from $n_{ZnO}/1$ to $n_{ZnO}/1.683$ The simulation in Figure 5d demonstrates that the hexagonal ZnO plays as an inner active microcavity while the PVK layer acts as a outer passive cavity. The stimulated emission puts out from the six corners of the active cavity, and some parts of modes resonate in the passive cavity again. It results in the lasing intensity are decreased properly because of the optical loss of PVK, but the Q factor is improved.

4. CONCLUSIONS

In summary, four configurations of WGM microcavities are designed to study the relationship between the WGM lasing behaviors and the medium around the ZnO microrod. The practical samples were fabricated by asymmetrically coated PVK on ZnO microrod. The lasing performances, such as, threshold, emission intensity, mode numbers, and Q factors were modulated and improved by the enhancement of the relative refractive index at side surfaces of the ZnO microrod because of the improvement of the net optical gain related to the TIR efficiency at the microcavity boundary. The typical mode equation, which was only suitable for WGM microcavity with homogeneous structure was also modified for general situation by considering the phase shift generated each side with various medium. The numerical simulation according to the modified equation provided nice-matched lasing modes and the corresponding mode serial numbers with the experimental data. The 2-dimensional FDTD simulation on the optical field distribution is also consist with the experiment observation for TE modes of the four configurations. This study is significant to design optically and electrically pumped WGM laser, especially to regulate the lasing performance by selecting the medium on the resonant microcavity surface.

AUTHOR INFORMATION

Corresponding Author

*E-mail: xcxseu@seu.edu.cn.

Notes

The authors declare no competing financial interest.

ACKNOWLEDGMENTS

This work was supported by "973" Program (2011CB302004), NSFC(60976002), RFDP (20110092130006), and JSIS (BE2012164).

REFERENCES

(1) Bagnall, D. M.; Chen, Y. F.; Zhu, Z.; Yao, T. *Appl. Phys. Lett.* **1997**, *70*, 2230−2232.

(2) Czekalla, C.; Sturm, C.; Grund, R. S.; Cao, B. Q.; Lorenz, M.; Grundmann, M. *Appl. Phys. Lett.* **2008**, *92*, No. 241102.

(3) Dai, J.; Xu, C. X.; Wu, P.; Guo, J. Y.; Li, Z. H.; Shi, Z. L. *Appl. Phys. Lett.* **2010**, *97*, No. 011101.

(4) Chen, R.; Ling, B.; Sun, X. W.; Sun, H. D. *Adv. Mater.* **2011**, *23*, 2199−2204.

(5) Zhu, H.; Shan, C. X.; Yao, B.; Li, B. H.; Zhang, J. Y.; Zhang, Z. Z.; Zhao, D. X.; Shen, D. Z.; Fan, X. W.; Lu, Y. M.; Tang, Z. K. *Adv. Mater.* **2009**, *21*, 1613−1617.
(6) Tian, Y.; Ma, X. Y.; Li, D. S.; Yang, D. R. *Appl. Phys. Lett.* **2010**, *97*, 061111.
(7) Liu, X. Y.; Shan, C. X.; Wang, S. P.; Zhang, Z. Z.; Shen, D. Z. *Nanoscale* **2012**, *4*, 2843−2846.
(8) Chu, S.; Wang, G. P.; Zhou, W. H.; Lin, Y. Q.; Chernyak, L.; Zhao, J. Z.; Kong, J. Y.; Li, L.; Ren, J. J.; Liu, J. L. *Nat. Nanotechnol.* **2011**, *6*, 506−510.
(9) Tang, Z. K.; Wong, G. K. L.; Yu, P.; Kawasaki, M.; Ohtomo, A.; Koinuma, H.; Segawa, Y. *Appl. Phys. Lett.* **1998**, *72*, 3270−3272.
(10) Dai, J.; Xu, C. X.; Sun, X. W. *Adv. Mater.* **2011**, *23*, 4115−4119.
(11) Vollmer, F.; Arnold, S. *Nat. Methods* **2008**, *5*, 591−596.
(12) Vollmera, F.; Arnoldb, S.; Kengb, D. *Proc. Natl. Acad. Sci. U. S. A.* **2008**, *105*, 20701−20704.
(13) Dai, J.; Xu, C. X.; Zheng, K.; Lv, C. G.; Cui, Y. P. *Appl. Phys. Lett.* **2009**, *95*, 241110.
(14) Dai, J.; Xu, C. X.; Ding, R.; Zheng, K.; Shi, Z. L.; Lv, C. G.; Cui, Y. P. *Appl. Phys. Lett.* **2009**, *95*, 191117.
(15) Tung, F. K. L.; Ma, N.; Poon, A. W. *Proc. SPIE* **2003**, *5116*, 488−494.
(16) Zhang, C. F.; Zhang, F.; Sun, X. W.; Yang, Y.; Wang, J.; Xu, J. *Opt. Lett.* **2009**, *34*, 3349−3351.
(17) Wiersig, J. *Phys. Rev. A* **2003**, *67*, 023807.
(18) Nobis, T.; Grundmann, M. *Phys. Rev. A* **2005**, *72*, 063806.